Steels," in Volume 4, eighth edition, of the *Welding Handbook, Materials and Applications, Part 2*.[16]

Austenitic stainless steels can be readily welded with fusion processes, but may have problems with hot cracking and distortion in large sections. The friction stir welding of these materials requires the use of tools made of W, W-Re, or PCBN using higher forces and slower travel speeds relative to Al alloys.[17] Peak stir-zone temperatures have not been reported, but likely exceed 1000°C (1832°F). As with most high-temperature materials, tool wear and deformation is a problem with metallic tools, while the service life of CBN tools may be limited by their low toughness.

Results of one study revealed that the stir zone of these welds was characterized by a refined grain size with equiaxed grains due to dynamic recrystallization. The stir zone also exhibited a banded region on the advancing side of the weld, often called the *swirl zone*. The formation of sigma phase has been confirmed in these bands by TEM examination with a local loss in corrosion properties. The accelerated formation of sigma phase was attributed to the intense deformation that occurred locally during friction stir welding. Microhardness results normally showed relatively flat profiles across all of the weld zones. Tensile results indicated increased yield strength and tensile strength with respect to the base metal, with a slight loss in elongation to failure.

A few studies were completed on the friction stir welding of duplex and ferritic stainless steels using cubic boron nitride tools, with the result that the ferritic alloy showed increased stir-zone hardness, suggesting the formation of martensite.

HEAT TRANSFER IN FRICTION STIR WELDS

The thermal cycles experienced by the material in and around the weld area have a profound influence on the final microstructures, mechanical properties, residual stresses and distortion of the weldment. Key features of the local thermal cycle that have the greatest effect include the peak temperature and the cooling rate. In this section, various models that have been used to simulate heat flow and thermal cycles during FSW are reviewed. Published research on experiments involving temperature measurements during FSW also are examined.[18]

MODELING OF HEAT TRANSFER

As a first approximation, temperature distribution around the FSW tool when welding thin plate can be calculated using Rosenthal's equation for moving-point heat source. As with laser beam welding or arc welding, the temperature contours are parabolic, compacted ahead of the tool and expanded behind it. However, the heat generation is not localized to a small area in a friction stir weld. It occurs over the entire interface between the tool and the workpiece. The thermal field is inherently asymmetric along the centerline of the weld due to differences in heat generation between the advancing and retreating sides. Hence, heat flow inherently is three dimensional. In addition, heat is carried by the considerable plastic flow that takes place around the tool, and consequently, heat transfer is both conductive and convective. Figure 7.19 shows computed temperature profiles in the X-Z, Y-Z and X-Y planes for a friction stir weld on AA6061 using an H-13 tool, with a pin radius of 6 mm (0.24 in.) and a shoulder radius of 25 mm (1 in.). The axial pressure was 12.7 MPa (1.842 ksi). The welding velocity was 1.59 mm/s (0.063 in./s) and the tool rotational speed was 344 rpm. The asymmetry in temperature distribution was not pronounced because of the high thermal conductivity of aluminum.

To understand heat transfer during friction stir welding, the heat generation must be quantified. Heat generation depends on the dynamics of the interface between the tool and the workpiece. A better understanding of heat generation and heat transfer in FSW has evolved over the years and is best represented by the increasing sophistication of numerical models for FSW.

Initial models for friction stir welding were analytical and were based on models for rotary friction welding. Local heat generation rate was a product of tool rpm, axial pressure, distance from the axis, and an effective coefficient of friction, μ. In one model, a value of two was chosen for μ, based on results from rotary friction welding experiments, and the thermal properties of the workpiece were assumed to be independent of temperature. The heat source was constructed by integrating the Rosenthal equation, using a series of point sources symmetrically disposed around the periphery of the shoulder. The model inherited the temperature singularity at the shoulder periphery from the Rosenthal formulation.

16. American Welding Society (AWS) Welding Handbook Committee, W. R. Oates and A. M. Saitta, ed., 1988, *Welding Handbook, Materials and Applications, Part 2*, eighth edition, Volume 3, Chapter 5, Miami: American Welding Society.

17. The titles, authors, and facts of publication of technical papers and other resources represented in this section are listed in the Bibliography in the Stainless Steel Alloys section.

18. The titles, authors, and facts of publication of technical papers and other resources represented in this section are listed in the Bibliography in the Heat Transfer section.

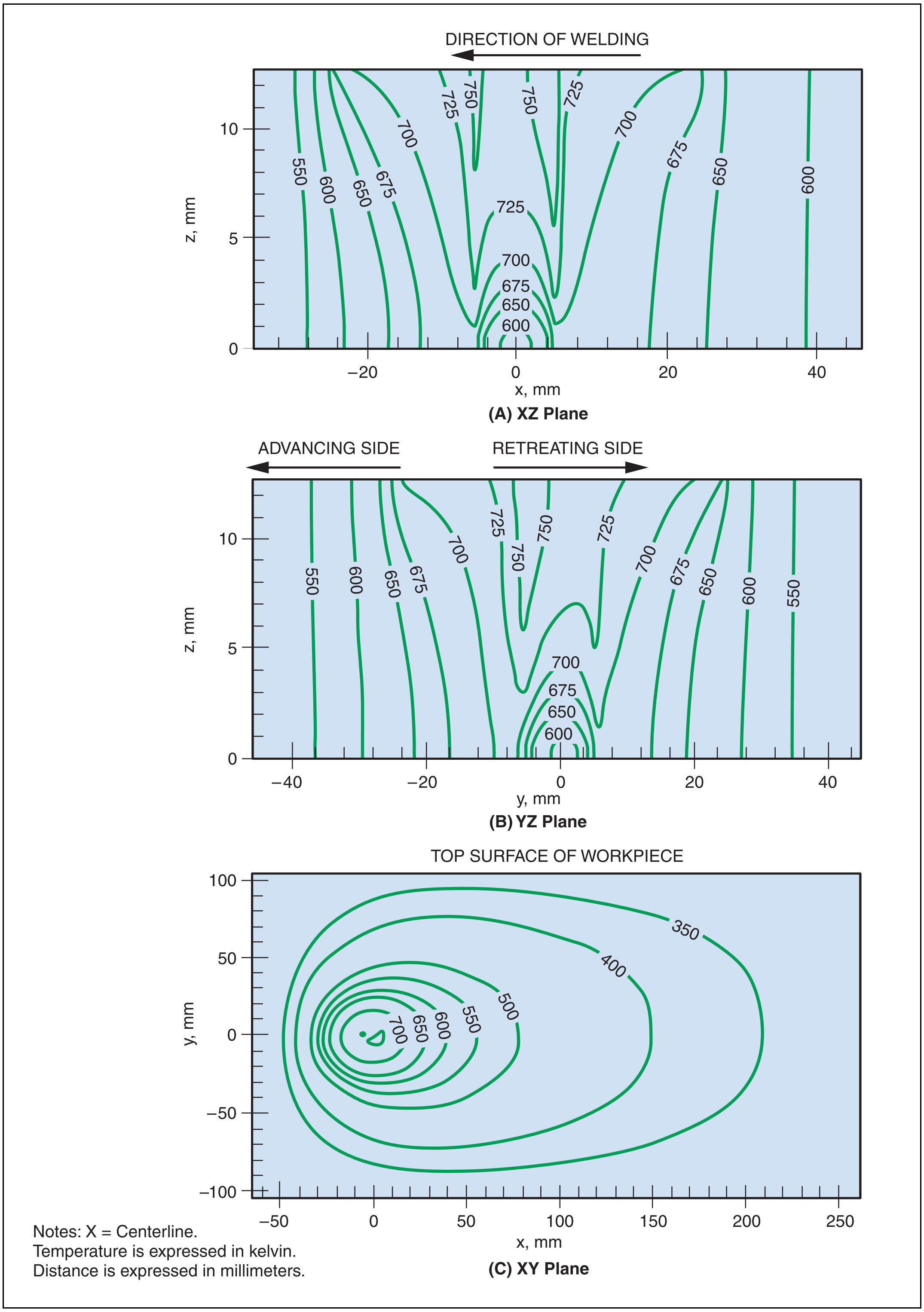

Source: Adapted from Nandan, R., G. G. Roy and T. DebRoy, 2006, Numerical Simulation of Three-Dimensional Heat Transfer and Plastic Flow During Friction Stir Welding, *Metallurgical and Materials Transactions A*, 37(4): 1247–1259.

Figure 7.19—Temperature (K) Distribution Profiles for a Friction Stir Weld on AA6061 at (A) XZ Plane, (B) YZ Plane, and (C) XY Plane

Mass flow, heating effects from the pin, and heating due to visco-plastic dissipation were not considered in this model. Nonetheless, the model confirmed that temperature distribution in friction stir welding is a function of tool rpm, axial pressure, shoulder radius, and the thermal properties of the workpiece material.

A modification of this model included the heating effect of the entire shoulder by integrating the area from the pin radius to the shoulder radius. The product of the coefficient of friction, μ, and the pressure, P, (μ × P) was adjusted to obtain the temperature at the weld centerline corresponding to thermocouple measurements. Like the previous model, this model did not consider mass flow, heating effects from the pin, and heating due to visco-plastic dissipation.

However, this approach using a coefficient of friction is too simplistic and is not adequate. Hence, in a subsequent model, a state variable, δ, was introduced to describe three different tool and workpiece contact conditions: sticking ($\delta = 1$), sliding ($\delta = 0$) and sticking and slipping ($0 < \delta < 1$). Heating effects from both the shoulder of the tool and the pin were included to ensure that the model was physically realistic. Heat generation for the sliding condition was based on a friction-heating approach previously described. Heating for the sticking condition was based on the assumption that the workpiece material shears and hence the stress in the workpiece in contact with the tool is equal to the shear stress for yielding at the welding temperature. Heat generation for the stick-and-slip condition was assumed to be a linear combination of the two, with δ describing the fraction of sticking. Results of the model suggested that the tool shoulder contributed 86% of the total heating, the vertical surface of the pin contributed 11% of the total heating, and the pin tip contributed 3% of the total heating. Comparison of modeling results to experimental results indicated that the conditions during friction stir welding most closely matched the sticking condition in 2024 aluminum alloy.

Since analytical equations are only approximations, several full numerical solutions using both finite-volume and finite-element techniques were obtained for the conduction equations in FSW. In these models, a steady assumption was made for the weld period, and heat generation at the tool-workpiece interface was simulated using a moving heat source.

Conductive and Convective Heat Transfer

Since large-scale plastic deformation occurs near the tool, heat transfer near the tool is predominantly convective. Hence, the effects of deformation must be taken into account for more accurate modeling. Primarily, there are two approaches to model deformation. One is to use solid mechanics, which involves finite-element analysis in most cases. Another approach is to treat the deformation as visco-plastic flow of high viscosity material; this falls under the purview of computational fluid dynamics (CFD) problems. Deformational heating (in solids) or viscous dissipation (in fluids) within the workpiece should be taken into account apart from interfacial heating, which was considered in heat-conduction models.

Computational Fluid Dynamics Models

The computational fluid dynamics models have evolved from simple two-dimensional to comprehensive three-dimensional models able to predict asymmetry of the thermal fields with respect to the joint line. One early CFD effort used a two-dimensional visco-plastic model for aluminum alloy based on laminar, viscous, and non-Newtonian flow around a circular cylinder. The non-Newtonian viscosity based on the constitutive equations for aluminum was calculated. One of the important observations was that beyond the rotational zone immediately adjacent to the FSW tool, the material transport occurred mainly along the retreating side.

Material flow also has been modeled using commercial CFD software, FLUENT.[19] Complex tool geometries were benchmarked for mechanical efficiency during the friction stir welding of a 7075 Al alloy. A triangular tool with convex surfaces, such as Trivex™ and a conventional tool, such as Triflute™ were compared by examining the streamlines around these tools.[20]

Two-dimensional models do not consider the vertical mixing during friction stir welding, which is observed experimentally. A comprehensive three-dimensional heat and material flow model solving the equations of conservation of mass, momentum, and energy, with appropriate boundary conditions and employing spatially variable thermal-physical properties and non-Newtonian viscosity has been shown to reliably predict heat transfer and plastic flow in friction stir welds of different systems, like aluminum alloys, mild steels, and stainless steels.

Solid-Mechanics Models

An approach based on solid mechanics, assuming a rigid visco-plastic material where the flow stress depended on strain rate and temperature, also has been used to model friction stir welding. The heat generation rate, expressed as the product of the effective stress and the effective strain rate, provided the boundary condition for calculation of temperature distribution in the workpiece and the tool, using a three-dimensional finite analysis code.

19. Computational fluid dynamics simulation software, Canonsburg, Pennsylvania: FLUENT.
20. Trivex and Triflute are trade marks of TWI.

One practical application involved the use of solid-mechanics-based models with adaptive boundary conditions for void-free welds. A fully coupled thermomechanical three-dimensional finite-analysis model was developed using the FE package ABAQUS[21] with material flow modeled using Johnson-Cook law. The contact forces were modeled by Coulomb's Law of friction. Results of the simulations indicated that the development of the sticking contact condition at the pin-workpiece interface is important for the success of processes involving recoalescence at the rear of the tool. The key to producing defect-free welds is the development of a high-temperature region close to the tool-workpiece interface surrounded by a zone of stiffer material at lower temperature.

Shock-Wave Model

An Eulerian shock wave physics code also has been used to model friction stir welding in aluminum. The three-dimensional code solves time-dependent equations for continuum mechanics and is well suited for modeling very large deformations at high strain rate, such as in a ballistic impact. The model predicted peak temperatures near 500°C (932°F) under the shoulder adjacent to the pin, where the largest deformation gradients were found. It should be noted that this result contrasts with those of other researchers who found peak temperatures near the shoulder periphery due to the greater relative local tool velocity.

Other Models

A force-balance approach has been employed to determine temperature profiles during friction stir welding; however, temperature fields found in this research were erroneous. Uncertainties in thermal conductivity were cited as possible causes for the discrepancy.

A model based on the torque input was also developed for friction stir welding. This model used the tool rotational speed and a shear stress of 14 MPa (2.03 ksi) in conjunction with tool dimensions to estimate the heat flux with and without backing plates by employing suitable convective heat transfer coefficients. Model results showed close qualitative agreement with measurements.

EXPERIMENTAL OBSERVATIONS OF TEMPERATURES

Many experiments aimed at determining temperatures at various locations of friction stir welds have been reported. Most of the experiments have involved thermocouple measurements. In this section, selected thermocouple measurements are discussed along with a method to infer peak temperatures in Al alloys from microstructural observations.

Thermocouple Measurements

In one study, peak welding temperatures reported during friction stir welding experiments on Al alloys were less than the solidus temperature of the alloy. Readers may wish to refer to the section on phase diagrams in Chapter 4 of Volume 1 of the *Welding Handbook,* ninth edition, for further discussion of the solidus temperature.[22] Peak temperatures of ~450°C (~842°F) were measured for the stir zone of friction stir welds made at 400 rpm on 6.4-mm (0.25-in.) 6061 aluminum. Figure 7.20 shows representative thermal cycles. Peak temperatures in the stir zone near the pin were nearly isothermal, and the peak temperature gradient through the plate thickness was small. No temperature difference was found between the advancing sides and the retreating sides. Peak temperatures were found to increase with increasing tool rpm and increasing tool pressure.

In another study, peak temperatures of 475°C (887°F) were reported near the boundaries of the stir zone and TMAZ in 7075 aluminum. Temperatures in the heat-affected zone ranged from 250°C (482°F) to 475°C (887°F), causing overaging and coarsening of the strengthening precipitates. (Refer to Figure 7.11 for an illustration of the weld zone microstructures, precipitate distributions, and temperature ranges for a friction stir weld on 7075 aluminum.)

In-Situ Inferences of Temperature

The θ (Al_2Cu) particles present in 2219 aluminum were used as in-situ sensors for eutectic melting to bound temperatures during the friction stir welding of this aluminum-copper alloy. This alloy contains at least 6.3% copper, which is above the maximum solid solubility for this system. The eutectic temperature for this system is 548°C (1018°F). No evidence of eutectic melting was observed in the stir zone or the TMAZ of these welds, confirming that peak temperatures were below the eutectic temperature and that no liquid phases existed during friction stir welding.

21. ABACUS, a finite element analysis program, Providence, Rhode Island: ABAQUS.

22. American Welding Society (AWS) Welding Handbook Committee, C. L. Jenney and A. O'Brien, ed., 2001, *Welding Handbook,* 9th ed., *Welding Science and Technology*, Vol. 1, Chapter 4, Miami: American Welding Society.

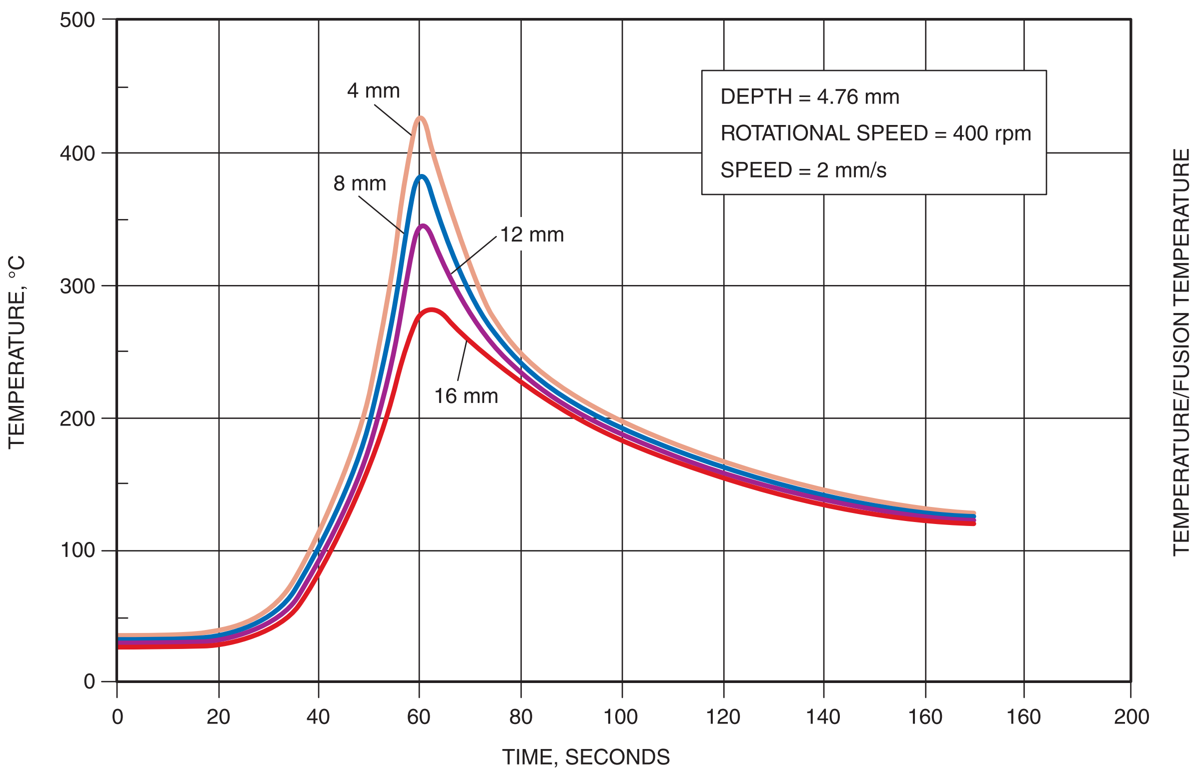

Source: Adapted from Tang, W., X Guo, J. C. McClure, L. E. Murr, and A. C. Nunes, 1988, *Journal of Materials Processing & Manufacturing Science* (USA), Vol. 7, No. 2 (10): 163–172.

Figure 7.20—Heat Input and Temperature Distribution in Friction Stir Welding on 6061 Aluminum

MATERIAL FLOW IN FRICTION STIR WELDING

Friction stir welding involves the movement of considerable amounts of viscous material around the tool followed by recoalescence of material near the back surface of the tool. An understanding of material flow during FSW is important for at least two reasons. First, welding conditions that produce certain undesirable flow patterns may result in the formation of discontinuities such as "wormhole" discontinuity.[23] Second, moving material also carries heat and may impact the thermal cycle. Models aimed at an improved understanding of material transport are discussed in the first part of this section. Subsequently, experimental observations of material flow associated with friction stir welds are reviewed.[24]

MODELING OF MATERIAL FLOW

In one set of simulations, the flow patterns around a friction stir welding tool were modeled using numerical solutions of coupled Navier-Stokes and heat transfer equations. The heat source was modeled by considering viscous dissipation of mechanical energy. Results of the simulations suggest that the following three distinct flow regimes exist as a function of distance from the shoulder:

1. A region of rotation just under the shoulder, where flow occurs in the direction of tool rotation;

23. The term *wormhole* as used in friction stir welding is a mechanical lack-of-bonding cavity discontinuity and is not to be confused with the nonstandard term *wormhole porosity* (elongated piping porosity) used with gas-shielded arc welding processes.

24. The titles, authors, and facts of publication of technical papers and other resources represented in this section are listed in the Bibliography in the Material Flow section.

2. A region near the base of the pin, where material is extruded past the pin; and
3. A transition area between the two regions, where flow is chaotic.

Of particular interest in the transition area was the report of an unstable region, in which flow reversal occurred at a location where the rotational and translational velocities of the tool were equal in magnitude and opposite in direction.

Solid-mechanics models also have been used to analyze the deformation of plasticized metal during friction stir welding. One solid-mechanics model was developed to analyze the flow of material during friction stir welding. This model closely reproduced the experimental marker studies that used dissimilar Al alloy markers, as discussed below. Results of the simulations also suggested that material tended to pass mainly around the retreating side of the pin.

Streamline plots of velocity obtained using a CFD technique gave insight into the nature of material flow around the tool pin. The pattern of streamlines plotted in Figure 7.21 illustrates a tool moving to the right and rotating in a counterclockwise direction when viewed from above. The streamlines show the paths taken by the material as it flows around the pin and is re-coalesced behind the pin. The streamlines split in front of the pin on the advancing side. Material within the shoulder diameter was transported around the retreating side of the pin in the direction of rotation, following arched paths shaped like concentric horseshoes (or the Greek letter "Ω"). The streamlines subsequently rejoined behind the pin on the advancing side.

The material that passed around the retreating side of the pin was deposited behind the pin in the same lateral position relative to the joint line as it originated. Consequently, the material originally located far on the advancing side (but within the pin diameter), was transported a greater distance than the material initially located closer to the retreating side, and thus experienced greater strains. Since the same material traveled a greater distance in the same time period (~1 revolution of the pin), it also was subjected to greater strain rates. In addition, results indicated that excessive rotational speeds (rpm) may allow some material to flow around the advancing side and that this condition may lead to the formation of incomplete bonding discontinuities.

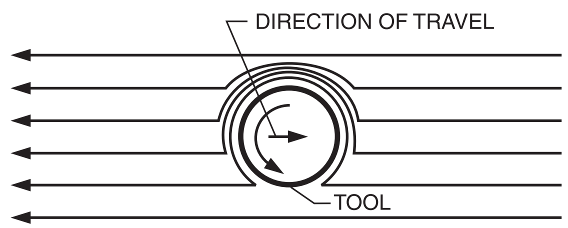

Notes:
The tool is represented by the solid ring in the center of the diagram.
Direction of tool rotation: counterclockwise when viewed from above.
The retreating side is at the top and the advancing side is at the bottom.

Source: Adapted from Seidel, T. U., and A. P. Reynolds, 2003, *Science and Technology of Welding and Joining*, Warrendale, Pennsylvania: The Minerals, Metals and Materials Society (TMS), 8(3): 175.

Figure 7.21—Plot of Streamlines Showing Metal Flow around the Friction Stir Welding Tool

EXPERIMENTAL OBSERVATIONS OF MATERIAL FLOW

Experiments with friction stir welds on both similar and dissimilar alloys between aluminum and copper and between different aluminum alloys have shown that the extensive plastic deformation during FSW creates complex vortex and swirl-like structures, especially near the interface of the weld zone and base metal. In welds of dissimilar aluminum alloys, striations and patterns of compositional difference were observed that corresponded to the spacing of the threads on the pin. The formation of these patterns was influenced by the geometry of the pin and the rotational speed.

Several researchers have used experimental tracer techniques to investigate the nature of plastic deformation and metal flow during friction stir welding. One investigation used steel shot markers placed at various plate depths and lateral distances from the weld centerline in an aluminum alloy. The position of the steel shot after welding was recorded using radiography. The markers initially placed near the top of the plate were lifted as they approached the tool and were deposited in a chaotic and random fashion behind the tool. Some of the material originally near the top surface subsequently was carried downward by the threads on the pin. Markers originally located near the mid-thickness of the plate also were lifted in front of the tool, and those positioned in the path of the pin were transported around the retreating side of the tool and deposited in the same lateral position relative to the centerline (refer to Figure 7.21). Markers positioned near the bottom of the plate passed under the pin without lifting.

Other efforts using markers in the form of plugs of dissimilar aluminum alloys with different responses to etching revealed that material was carried forward on the advancing side of the pin, and backward around the retreating side. In addition, the stir zone took on a more rounded shape when the diameter of the pin was increased, with the maximum stir-zone width occurring near the mid-thickness of the plate. The pin with the largest diameter produced a large bulge on the advancing side of the stir zone.

Composite markers of aluminum-silicon carbide (Al-SiC) and tungsten placed near the plate mid-plane on both the advancing and retreating sides also have been utilized. Results of this study showed that markers are lifted in front of the tool and subsequently carried downward by the threads. In addition, the markers initially on the advancing side were distributed over a wider region.

APPLICATIONS

Friction-stir welding has focused mainly on aerospace and marine applications, with a growing number of applications in the automotive, marine, and rail transportation industries. Some of the aerospace and aircraft projects include construction of the main fuel tank of the space shuttles, the booster core tanks of Delta rockets, floor decking for the C-17 Globemaster cargo aircraft, and fuselage and wing sections of the Eclipse 500 Business Class jet. Marine and rail transportation applications include the welding of fast-ferry decking and sections of subway and rail cars.

The first commercial application of friction stir welding was the joining of 20-m (65.6-ft) sheets of aluminum for the construction of fast ferries in Norway. In the United States, the Boeing Company was the first to use the friction stir welding process, developing its own technology and standards and cooperating with government, university, and industry resources to implement the construction of the Delta series of aerospace launch vehicles. The booster core of the Delta IV, or first-stage launch vehicle, includes a liquid oxygen tank 12-m (44-ft) high, an 8.4-m (28-ft) high fuel tank and a 4.8-m (216-ft) high inter-stage cylinder welded with friction stir welding. Figure 7.22(A) shows a weld qualification tank during production. The tanks are formed using three sheets of 22.22-mm (7/8-in.) thick 2014-T6 aluminum alloy. Tank panels are positioned for welding from the inside, as shown in Figure 7.22(B). Figure 7.22(C) shows the friction stir weld in progress.

Several aircraft builders use friction stir welding, including Eclipse Aviation and Airbus. Airbus used the friction stir process for their models A350, A340-500 and A340-600. Figure 7.23 shows the circumferential aluminum fuselage stiffeners and door doublers of

(A) Weld Qualification Tank in Production

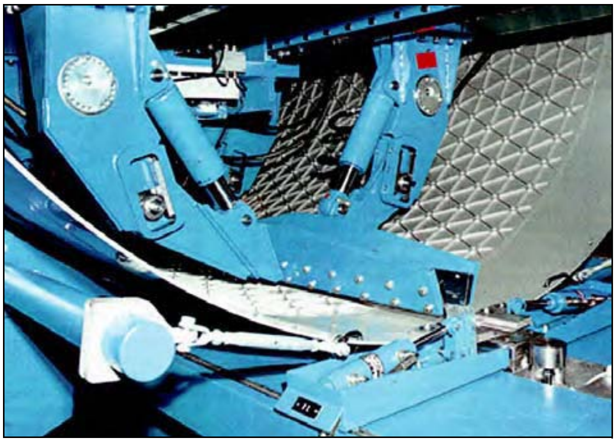

(B) Tank Panels Positioned for Welding from the Inside

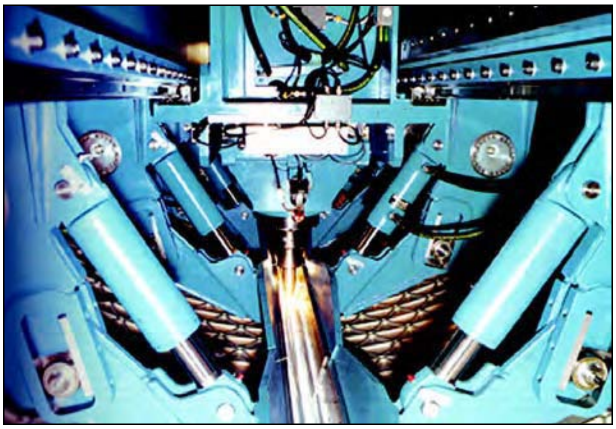

(C) The Friction Stir Weld in Progress

Photographs courtesy of the Boeing Company

Figure 7.22—Friction Stir Welding of 22.22-mm-Thick (7/8 in.) 2014-T6 Aluminum Alloy Panels for the Booster Core Tank of a Space Launch Vehicle

(A) (B) (C)

Photographs courtesy of Eclipse Aviation

Figure 7.23—(A) The Eclipse Jet with (B) Circumferential Aluminum Fuselage Stiffeners and (C) Door Doublers Attached with Friction Stir Welding

the Eclipse Business Class jet attached by friction stir welding.

Automotive applications of friction stir welding include suspension components and auto body weldments. Friction stir welding is used for these weldments because it does not react adversely to the coating used for this type of assembly. The Ford Motor Company has used the process to weld the central tunnel assembly of several thousand Ford GT automobiles. The Mazda Motor Corporation used friction stir spot welding to manufacture the automobile doors shown in Figure 7.24.

MECHANICAL PROPERTIES OF FRICTION STIR WELDS

Table 7.1 presents tensile data for base metal and friction stir weld samples in the transverse orientation for a number of common aluminum alloys.[25] The alloys

25. From a database compiled by T. J. Lienert. Base metal properties from ASM Metals Handbook. Materials Park, Ohio: ASM International.

(A) Door Structure Spot-Welded for Impact Stability

(B) Construction Detail

Photographs courtesy of Mazda Motor Corporation

Figure 7.24—Friction Stir Spot Welds in an Automobile Door

are listed along with their original temper conditions before welding. Yield strength, ultimate tensile strength and the percentage of elongation are provided for the base metal and friction stir weld metal for each alloy. Data for the friction stir welds were taken from reports in open literature and compiled into a database. Friction stir weld properties are shown for the average, standard deviation, and the number of data points (number of welds or tests) used to calculate the average and standard deviation for each alloy.

Comparisons of base metal and weld metal data for a given alloy indicate that yield and tensile strengths for friction stir welds generally exceed 60% to 70% of the yield and tensile strengths of the base metal. It should be noted that the strength data covers a considerable time span and includes data generated early in the development of friction stir welding. Markedly better results can be achieved with current tool designs and modern FSW machines that are stiffer and allow faster tool travel rates and lower heat input.

Referring to Table 7.1, it can be noted that the percent elongation for friction stir welds is always less than the values reported for the base metal. The lower values for friction stir welds (and nearly all welds in general) result from non-uniform elongation in the gauge length during testing. In turn, non-uniform elongation results from differences in microstructure across the weld region, and differences in microstructure result from variations in local thermomechanical histories developed during welding. In aluminum alloys, most of the strain during tensile testing is carried by the heat-affected zone. Partitioning of the strain across smaller lengths shows that the heat-affected zone actually undergoes considerable elongation. Hence, the low elongation values are artificial and should be viewed with these caveats in mind. As an example, Figure 7.25 shows the distribution of strains across the weld region for a tensile sample of a friction stir weld made on 7075-T6. The stir zone and base metal (not shown) undergo little straining, while the heat-affected zone carries considerable strain.

Fatigue data collected for friction stir welds is rather limited. Most fatigue studies have focused on aluminum alloys. In general, friction stir welds perform better in fatigue than fusion welds on the same material, but do not perform as well as that of the base metal. Figure 7.26 presents fatigue data for a friction stir weld on a 2024-T351 aluminum alloy. The testing was performed at a constant stress ratio of 0.1 and stress ranges up to 350 MPa (50.76 ksi).

Data for base metal and tensile properties of friction stir welds for three titanium alloys are presented in Table 7.2. Values are given for commercially pure Ti, the Ti-6Al-4V (Ti-6-4) alloy, and the Ti-15-3 alloy. In Table 7.2, the average standard deviation and number of data points used were included in the friction stir weld data where available. The loss of tensile properties in titanium alloys due to welding is much less than the loss incurred when welding aluminum alloys. These differences stem from the differences in the strengthening mechanisms between titanium and aluminum alloys. In other words, high-yield-strength and high-tensile-strength joint efficiencies can be achieved in Ti alloys with friction stir welds. In certain cases, the joint efficiency may appear to be greater than 100%. It should be noted that the caveats discussed previously for percentage of elongation also apply to titanium alloys.

Table 7.1
Test Data for Tensile Properties of Base Metals and Friction Stir Welds for Common Aluminum Alloys

Base Metal—Typical Properties*					Friction Stir Welds—Sample Properties								
					Yield Strength			Ultimate Tensile Strength			%Elongation		
Alloy	Original Temper	Yield Strength MPa (ksi)	Ultimate Tensile Strength MPa (ksi)	% Elongation	Average MPa (ksi)	Standard Deviation MPa (ksi)	Number of Data Points	Average MPa (ksi)	Standard Deviation MPa (ksi)	Number of Data Points	Average	Standard Deviation	Number of Data Points
2014	T6	414 (60)	483 (70)	13	243 (35.2)	25 (3.6)	2	355 (51.4)	36 (5.2)	9	N/A	N/A	N/A
2024	T3	345 (50)	483 (70)	18	308 (44.7)	34 (5)	15	416 (60.4)	27 (3.9)	23	7.8	3.8	14
2195	T8	N/A	N/A	N/A	253 (36.7)	10 (1.5)	29	396 (57.5)	11 (1.6)	35	8.5	1.6	33
5083	O	145 (21)	290 (42)	22	132 (19.1)	7 (1)	4	306 (44.4)	19 (2.8)	15	22.5	0.7	2
5454	O	117 (17)	248 (36)	22	101 (14.6)	8 (1.1)	3	245 (35.5)	17 (2.4)	5	18.9	4.4	5
5454	H32/H34	207 (30) 241 (35)	276 (40)/ 303 (44)	10	119 (17.3)	8 (1.1)	9	251 (36.4)	9 (1.3)	9	19.6	3.8	9
6013	T4	145 (21)	276 (40)	20	191 (27.7)	40 (5.8)	3	306 (44.4)	12 (1.8)	3	4.8	3.1	3
6013	T6	303 (44)	365 (53)	5	265 (38.5)	46 (6.6)	5	316 (45.9)	21 (3.1)	5	6.4	1.4	3
6061	T6	276 (40)	310 (45)	17	161 (23.4)	48 (6.9)	7	221 (32.1)	23 (3.3)	13	10	3.4	7
6082	T4	N/A	N/A	N/A	119 (17.2)	23 (3.3)	5	211 (30.6)	32 (4.6)	7	14.5	6.2	5
6082	T6	262 (38)	310 (45)	6	150 (21.7)	10 (1.4)	8	238 (34.6)	12 (1.7)	9	10.2	6.1	8
7050	T73/T7451	434 (63)	496 (72)	12	444 (64.4)	63 (9.1)	6	473 (68.6)	45 (6.5)	11	6.5	0.5	6
7075	T651	503 (73)	572 (83)	11	334 (48.4)	16 (2.3)	3	439 (63.6)	30 (4.3)	7	5	2.1	3
7075	T73	393 (57)	474 (69)	7	N/A	N/A	N/A	444 (64.4)	54 (7.8)	4	N/A	N/A	N/A

Notes:
— The test configuration was in the transverse orientation.
— N/A = Not available for this table.
— Standard deviation normally applies only to Gaussian distributions and is applicable only for distributions with sample sizes greater than 8; however, standard deviations are included in this table for small sample sizes to provide some indication of the distribution about the mean.

*Typical properties of base metals are from *ASM Metals Handbook*, Materials Park, Ohio: ASM International. Properties of 6013 and 6075 are from Aluminum Standards and Data, 2006, Aluminum Association. Properties of 6082 T6 are from ASTM B-209, ASTM International.

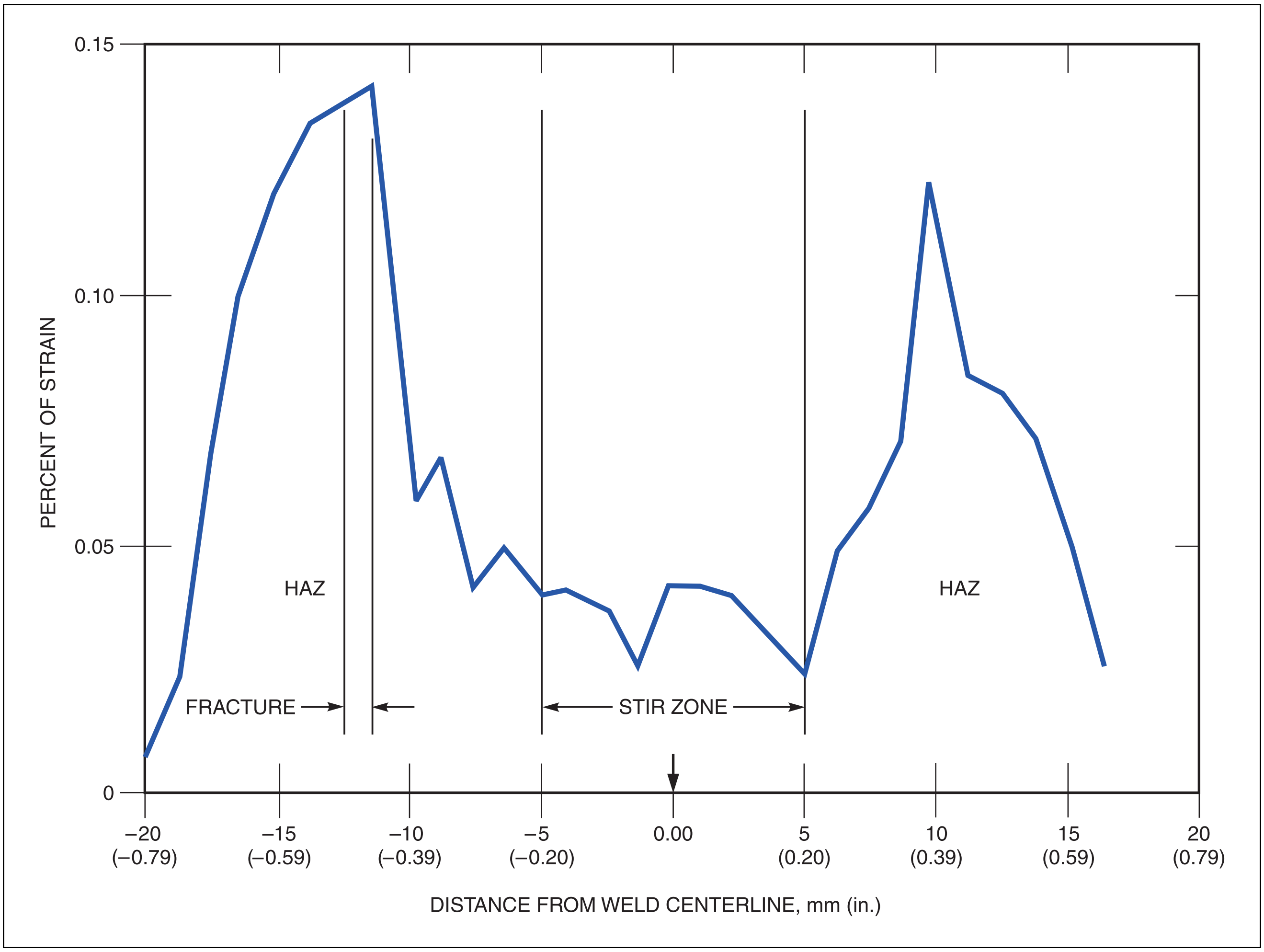

Source: Adapted from Mahoney, M. W., C. G. Rhodes, J. G., Flintoff, W. H, Bingel, and R. A. Spurling, 1998. Properties of Friction Stir Welded 7075-T651 Aluminum. *Metallurgical and Materials Transactions* 29A: 1955–1964.

Figure 7.25—Distribution of Tensile Strains Across the Weld Region in a Sample Friction Stir Weld in 7075-T651 Aluminum Alloy

Table 7.3 lists tensile data for the base metal and friction stir weld metal for 304 stainless steel and 2507 duplex stainless steel. The variations in base metal properties for the 304 alloys are believed to stem from differences in the amount of cold work. (These alloys are not heat-treatable.) It should be noted that the base metal for the 304 alloy has been tested in both transverse and longitudinal orientations. The average standard deviation and number of data points used are included in the friction stir weld data where available. Very good yield and tensile efficiencies can be achieved when welding stainless steel. Concerns discussed previously regarding the interpretation of percent elongation for friction stir welds also apply to stainless steels.

Acceptable yield and tensile joint efficiencies in steels can be achieved with friction stir welding. Tensile data for base metal and friction stir welds of several steels are reported in Table 7.4. The base metal for the DH-36 steel was tested in two orientations; the other steels were tested only in the transverse orientation. If base metal values were not available, minimum values were listed in this table. Charpy V-notch test data for friction stir welds on two steels are reported in Table 7.5.

Comparative data for this test were limited. In general, the average CVN data showed that friction stir welds in these steels provided acceptable toughness. However, in some cases, the scatter in the test data was large, and further study is required to understand the scatter.